Rock and Soil Mechanics

Volume 41 | Issue 9 Article 3

2-8-2021

Research on dynamic response characteristics of loess tableland slopes based on shaking table test

Fu-xiu LI
Key Laboratory of Loess Earthquake Engineering, Lanzhou Institute of Seismology, China Earthquake Administration, Lanzhou, Gansu 730000, China

Zhi-jian WU
College of Transportation Science &Engineering, Nanjing Tech. University, Nanjing, Jiangsu 210009, China, zhijianlz@163.com

Wu-jian YAN
Key Laboratory of Loess Earthquake Engineering, Lanzhou Institute of Seismology, China Earthquake Administration, Lanzhou, Gansu 730000, China

Duo-yin ZHAO
Chengdu Surveying Geotechnical Research Institute Co. Ltd. of MCC, Chengdu, Sichuan 610023, China

Custom Citation

LI Fu-xiu, WU Zhi-jian, YAN Wu-jian, ZHAO Duo-yin, . Research on dynamic response characteristics of loess tableland slopes based on shaking table test[J]. Rock and Soil Mechanics, 2020, 41(9): 2880-2890.

Rock and Soil Mechanics 2020 41(9): 2880−2890 ISSN 1000−7598
https: //doi.org/10.16285/j.rsm.2019.7060 rocksoilmech.researchcommons.org/journal

Research on dynamic response characteristics of loess tableland slopes based on shaking table test

LI Fu-xiu[1], WU Zhi-jian[2], YAN Wu-jian[1], ZHAO Duo-yin[3]

1. Key Laboratory of Loess Earthquake Engineering, Lanzhou Institute of Seismology, China Earthquake Administration, Lanzhou, Gansu 730000, China
2. College of Transportation Science &Engineering, Nanjing Tech. University, Nanjing, Jiangsu 210009, China
3. Chengdu Surveying Geotechnical Research Institute Co. Ltd. of MCC, Chengdu, Sichuan 610023, China

Abstract: Based on the typical loess plateau slope of Kongtong district, Pingliang city, a 1∶25 large-scale shaking table test is designed and accomplished using the conceptual model of the slopes with or without cracks. On the premise of satisfying the similarity principle, the dynamic response characteristics of model slopes of two kinds of structures are analyzed by inputting seismic waves in horizontal direction and vertical direction with different amplitudes. Results show that the horizontal and vertical seismic waves have obvious nonlinear amplification along the slope surface and the internal vertical direction, which reach the maximum value at the top of the slope. Under the horizontal seismic waves with the same amplitude, the acceleration amplification coefficient of the slope surface and section 4 are greater than that of the slope without crack at the same elevation in the middle and upper part of the slope, while in section 1, the amplification coefficient of the crack slope is smaller than that of the crack-free slope. After the seismic wave propagates through the slope soil, the predominant frequency changes significantly. With the increase of elevation, the slope will manifest selective amplification on middle and high frequency bands, which is more obvious on the side of fissure slope. Moreover, as the amplitude of seismic wave increases, the superior frequency transfers to the low frequency direction. However, the attenuation of predominant frequency is not obvious under the vertical seismic wave.

Keywords: loess tableland slope; shaking table test; crack; acceleration dynamic response; spectrum analysis

1 Introduction

China is a country with extensive geological hazards, especially in the western regions where tectonic movement is intense and strong earthquakes occur frequently. According to relevant records, there were 125 earthquakes and 285 corresponding collapses and landslides during 1216−1996, while 75% of the earthquakes and 77% of the collapses and landslides occurred in the western regions, causing a lot of road damage, bridge damage, house collapse and river blockage[1]. Such as the Huaxian earthquake in 1556, the Tianshui earthquake in 1654, the Tongwei earthquake in 1718, and the Haiyuan earthquake in 1920[2−6], these devastating earthquakes induced thousands of loess landslides, of which the loess plateau landslide is the most representative, resulting in significant economic losses and casualties. In addition, the mechanical erosion and chemical erosion caused by rainfall destroy the integrity of the slope. Therefore, it is very urgent to study the slopes on the loess tableland under earthquakes.

The center of China's infrastructure construction is gradually shifting to the western regions along with "The Belt and The Road" strategy and the rapid development of economy. The loess tableland has become more vulnerable under earthquakes with the continuous expansion of cities and the increase of human engineering activities. In order to better prevent and reduce disasters, it is necessary to study the deformation failure mechanism and response law of loess tableland slope under earthquakes. Presently, there are three methods to analyze the dynamic response of slopes: analytical method, numerical calculation method, and physical model test. Due to the discontinuity and inhomogeneity of the soil medium and the complexity of the slope dynamic response, it is very difficult to solve the dynamic response of slope by theoretical derivation. In addition, the dynamic response theory of slope is far from mature, its accuracy needs to be tested[6−7]. Loess is a type of granular media with special microstructure, which shows different mechanical properties under different amplitudes. Under the dynamic loading, the microstructure of loess gradually damages and deforms, which makes the macro properties of soil deteriorate continuously. However, the finite element software cannot simulate the evolution process of this deterioration, and the results from the numerical analysis need to be further verified by earthquakes or model tests[8]. In contrast, large-scale slope model using shaking

Received: 9 December 2019 Revised: 9 April 2020
This work was supported by the National Earthquake Science Joint Foundation of China(U1939209), the National Natural Science Foundation of China (41472297) and the Scientific Research Foundation for Introducing Talent of Nanjing Tech University.
First author: LI Fu-xiu, male, born in 1993. Master degree candidate, mainly working on the scientific research of geotechnical earthquake engineering. E-mail: 1225950800@qq.com.
Corresponding author: WU Zhi-jian, male, born in 1974. PhD, Professor, mainly working on geotechnical engineering and seismic engineering research E-mail: zhijianlz@163.com

tables are an important method to study the slope stability under earthquakes. Many scholars have obtained some meaningful results through shaking table test in the geotechnical engineering. Wu et al.[9] studied the failure process and acceleration response characteristics of pure loess slope with low water content and low slope angle under earthquake through shaking table test. Wang et al.[10] carried out the shaking table test on loess slope under the coupling effect of earthquake and rainfall and studied the dynamic response law. Zhang et al.[11] completed the centrifuge test with a scale of 1∶40, and systematically analyzed the seismic dynamic response laws and failure characteristics of loess-mudstone dual structure slope. The existing research on the dynamic characteristics of loess slope is of great significance for understanding the failure mechanism of loess slope under earthquake and guiding the anti-seismic design scheme. However, there are few research examples on the dynamic characteristics and stability analysis of slope on loess tableland, especially slopes with special structural surfaces(fissure). Therefore, it is of great significance to study the influence of fissures on the dynamic stability of loess tableland slopes. The current mainstream physical models include geotechnical centrifuges and large-scale shaking tables. For centrifuge test, the 1/n scaled rock and soil mass is placed in the ng (g is the acceleration of gravity) centrifugal field, and the centrifuge test can make the points in the model reach the in-situ stress level and reproduce the real dynamic characteristics. However, the geotechnical centrifuge test model is small and easy to be affected by the model size and boundary, and usually resulting in high operating cost. The shaking table model test is favored by scholars due to its relatively low cost and flexibility in changing the magnitude and direction of input amplitude[12−16].

This paper takes the typical fissure slope in Pingliang area as the prototype, and makes models of fissure slope and non-fissure slope to highlight the influence of fissure on slope response characteristics. Shaking table tests with a similarity ratio of 1∶25 were completed, and the tests reproduced the failure modes of two slopes under earthquake. Finally, this paper revealed the dynamic response characteristics of the slope on the loess tableland under different amplitude, and provided basis for the stability evaluation and the anti-seismic design scheme of slopes in this area.

2 Shaking table tests

2.1 Test equipment

The tests were carried out on a large-scale electric servo shaking table at the Key Laboratory of Loess Earthquake Engineering of the China Earthquake Administration. The size of the shaking table is 4 m × 6 m, driven by 28 servo motors, which can apply horizontal and vertical shaking. The maximum displacements in x and z directions are u_x = ± 250 mm and u_z = ± 100 mm, respectively. The frequency ranges in x and z directions are f_x = 0.1−70.0 Hz, f_z = 0.1−50.0 Hz. And the maximum accelerations are a_x = 1.7 g and a_z = 1.2 g, respectively. The shaking table and model box are shown in Fig. 1.

Fig. 1 Shaking table and model box

2.2 Prototype slope

In this test, the fissure slope in the loess tableland of Kongtong district was taken as the prototype in order to investigate the influence of fissure on the slope, a non-fissure slope with the same parameters was used as the contrast model. The prototype slope is 31.75 m× 35 m×25 m (length × width × height). Set up a shallow fissure and a deep fissure inside the slope. The length, width, and depth of the shallow fissure are 12.5 m, 0.075 m, and 5 m, respectively, and it is 2.5 m away from the shoulder of the slope. The length, width, and depth of the deep fissure are 25 m, 0.125 m, and 7.5 m, respectively, and it is 5 m away from the shoulder of the slope. Due to the slightly uneven terrain condition, the prototype slope is simplified accordingly, and the prototype slope and the simplified model are shown in Fig. 2.

2.3 Similitude design and boundary conditions

The generalized slope is a semi-infinite geological body with a certain slope and at least one side facing the air, theoretically, there is no boundary. However, in the model test, the soil can only be placed in a model box with finite scale, which will cause wave reflection at the boundary, inevitably produce the "model box effect", thus changing the vibration mode of the system, and maybe even causing secondary damage to the model slope[17]. Therefore, measures should be taken to mitigate the impact of the boundary. The general method that can be adopted is to add lining to the model box, change the box structure, materials, etc. In this test, a polystyrene foam sponge with a thickness of 5 cm was pasted on both sides of the vibration direction to absorb the energy at the boundary.

The main purpose of the designed model is truly reproducing the properties of the prototype slope, so it

(a) Prototype slope with fissures

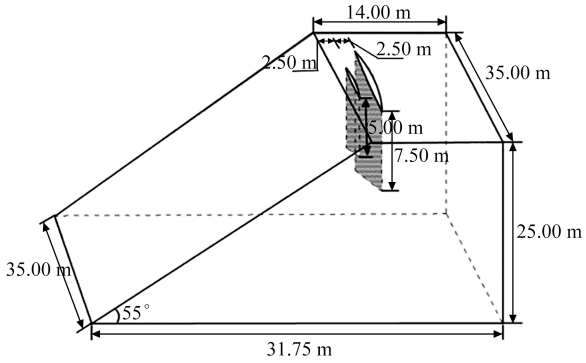

(b) Simplified model

Fig. 2 Prototype slope and simplified model

is necessary to use the similitude theory to guide the test. The similarity of model tests includes geometric similarity, kinematic similarity and dynamic similarity, and if the two physical quantities are similar in geometry and kinematic, they are also similar in dynamic. However, due to the complexity of the model and the limitation of the experimental conditions, it is difficult to meet the similarities of all parameters. Therefore, the main control parameters should be selected according to the test objective; and the secondary control parameters should be ignored. The test takes geometric size, material density, and acceleration of gravity as the major parameters. The similarity constants are $C_L = 25$, $C_\rho = 1$, $C_a = 1$ and the rest of the physical quantities are derived according to Buckingham theory and dimensional analysis[18−19]. The similar relationships are shown in Table 1.

Table 1 Similarity constants of model tests

Physical quantity	Similitude relationship	Similarity constant
Physical dimension: L	C_L	25.0
Density: ρ	C_ρ	1.0
Acceleration: a	C_a	1.0
Elastic modulus: E	$C_E = C_\rho C_l$	25.0
Cohesion: c	$C_c = C_\rho C_l C_a$	25.0
Internal friction angle: φ	C_φ	1.0
Time: t	$C_t = (C_l/C_a)^{1/2}$	5.0
Frequency: f	$C_f = (C_a/C_l)^{1/2}$	0.2

Note: C_L, C_ρ, C_a, C_E, C_c, C_φ, C_t, and C_f are the similarity constants of geometric dimension, density, acceleration, elastic modulus, cohesion, internal friction angle, time and frequency, respectively.

2.4 Preparation of the model slope

The prototype slope is mainly composed of Q_4 loess, and the theoretical values obtained using similitude theory has the characteristics of low elastic modulus and low cohesion. Therefore, the field soil cannot be used in the test, and it is difficult to replace the model soil with a certain material. The method of mixing various materials was used in this test in order to meet the requirements of similitude theory.

Considering the material characteristics, Q_4 loess was selected as the main material of the model soil, and the proper undisturbed soil was selected in the sampling process to avoid the loess with high salinity. In order to improve the purity of soil, soil with less impurities was selected as far as possible in the sampling process. Fly ash, barite powder and sawdust were auxiliary materials, water was binder material. Barite powder was mainly used as counterweight. Fly ash was a kind of non-cohesive elastic particles, which can reduce the cohesion. Sawdust can improve the internal friction angle of model soil. In order to ensure the continuity of particle gradation and avoid the influence of impurities, the loess and sawdust were sieved by 1.0 mm and 0.5 mm, respectively. The cohesion, internal friction angle, density and other parameters of the model soil were close to the target values by adjusting the content of materials, and were verified by direct shear test and triaxial test. Finally, the model material ratio was determined as follows: loess: barite powder: fly ash: sawdust: water was 0.50∶0.20∶0.21∶0.03∶0.06. The corresponding physical and mechanical parameters are shown in Table 2.

Table 2 Physical and mechanical parameters of soil

Type	Density ρ /(kN·m^{-3})	Cohesion c /kPa	Elastic modulus E /MPa	Internal friction angle φ/(°)
Actual value of prototype soil	1.36	22.27	72.00	14.5
Target value of model soil	1.36	0.89	2.88	14.5
Measured value of model soil	1.36	7.44	20.80	15.0

2.5 Making of the model and layout of sensors

The geometric similarity ratio between the model slope and the prototype slope is 1∶25. The scale of model slope is 1.4 m × 1.4 m ×1.1 m(length × width × height), and the slope angle is 55°. The left side slope is the fissure slope model in which the length of the shallow fissure is 50 cm, width of 3 mm, depth of 20 cm, and the length of the deep fissure is 100 cm, width of 5 mm, depth of 30 cm, the shallow and deep fissures are arranged 10 cm and 20 cm away from the slope shoulder, respectively. The specific dimensions are shown in Fig.3(a). The model slope was made in layers from bottom to top, and the

thickness of each compaction was controlled at 10 cm. In the process of laying, the compactness was used to control the construction quality. After each layer was laid, a ring knife tests were performed at 3 different positions on the surface to keep the density consistent with the prototype soil. The surface should be roughened to avoid unevenness after each layer of material was compacted. Two aluminum boards were placed in the corresponding positions to simulate the fissures of the prototype slope. The aluminum boards were wrapped with plastic film and coated with Vaseline until the model was filled in. After the model was constructed, the aluminum boards were manually pulled out after 24 h of maintenance.

A total of 40 acceleration sensors were arranged in the test, and all of them were arranged on the longitudinal section in the middle of the model. In order to compare and study the dynamic response characteristics of the two slopes, the principle of symmetrical arrangement was adopted, and an acceleration sensor A_0 was arranged on the table for later data checking. The acceleration sensor adopted were the EY5341 three-way capacitive sensors with a sensitivity of 680 MV / *g*, and a range of ± 2 *g*. The arrangement of acceleration sensor is shown in Fig.3(b).

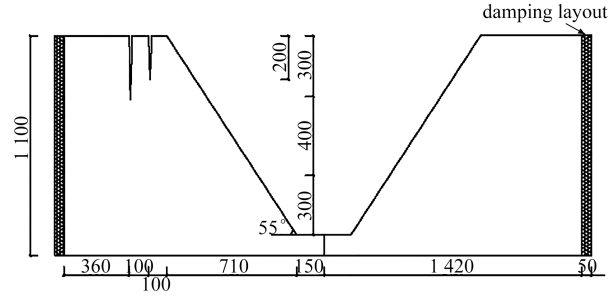

(a) Longitudinal section

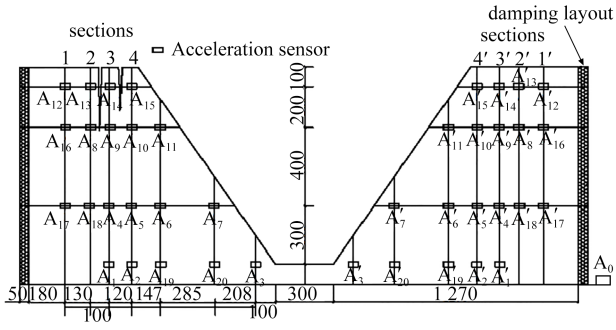

(b) Layout of acceleration sensor

Fig. 3 Longitudinal section of slope and layout of sensors (unit: cm)

2.6 loading input

The Wenchuan Tangyu earthquake motion and the El-Centro earthquake motion were scaled(5 times) according to the similarity ratios. The *x* direction and *z* direction were loaded according to magnitude of VI(corresponding ground acceleration 45−89 cm·s^{-2}) , VII (90−170 cm·s^{-2}), VIII (180−35 cm·s^{-2}), IX (36−700 cm·s^{-2}) in a step-by-step way.

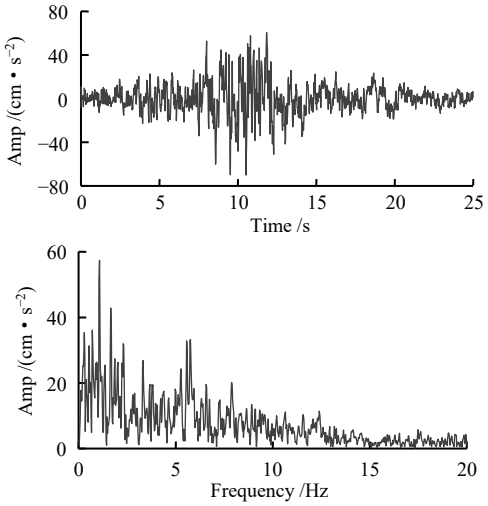

(a) Time history and spectrum of Wenchuan-Tangyu wave

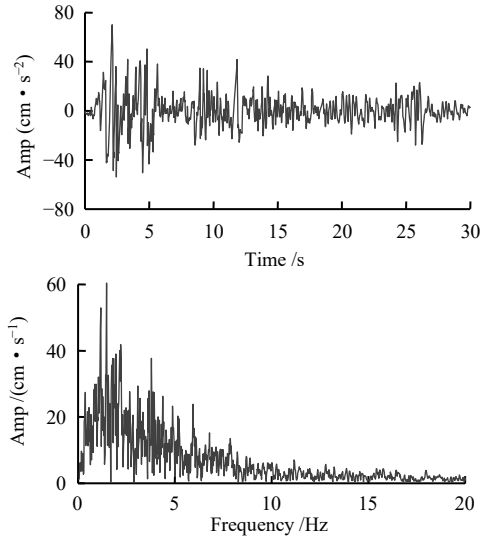

(b) Time history and spectrum of El-Centro wave

Fig. 4 Time histories and FFT of seismic waves

Table 3 Cases of loading test

Loading mode	Motion	Peak amplitude (cm • s^{-2})	Direction
1	Tangyu motion	54	Horizontal
2	El-Centro motion	35	Horizontal
3	Tangyu motion	54	Vertical
4	El-Centro motion	36	Vertical
5	Tangyu motion	95	Horizontal
6	El-Centro motion	65	Horizontal
7	Tangyu motion	138	Vertical
8	El-Centro motion	72	Vertical
9	Tangyu motion	195	Horizontal
10	El-Centro motion	153	Horizontal
11	Tangyu motion	311	Vertical
12	El-Centro motion	144	Vertical
13	Tangyu motion	355	Horizontal
14	El-Centro motion	320	Horizontal
15	Tangyu motion	476	Vertical
16	El-Centro motion	217	Vertical
17	Tangyu motion	517	Horizontal
18	El-Centro motion	475	Horizontal

3 Acceleration response analysis of slope

In the acquisition process, the measured acceleration wave will be affected by the sensor drift and the high frequency noise, such as the resonance of the model box. In order to eliminate these effects, the SeismSignal software is used to perform baseline correction for all acceleration(PGA) time histories with a band-pass filter of 0.1−40 Hz. Figure 5 shows the acceleration time histories of measuring points A_3, A_3', A_{15}, A_{15}' under the horizontal Tangyu motion with peak acceleration of 95 gal, it can be seen that the acceleration time histories of the monitoring points are similar and the amplification effect is very obvious.

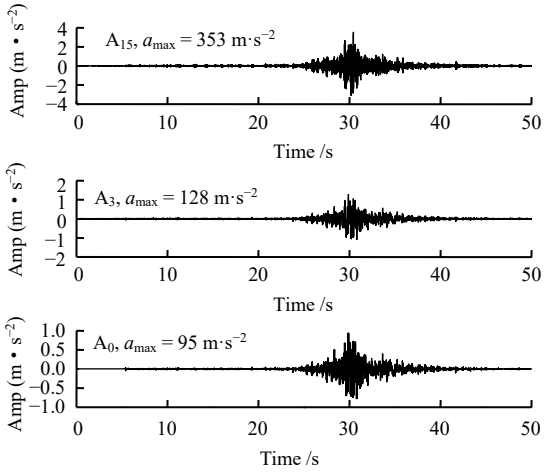

(a) Fissure slope

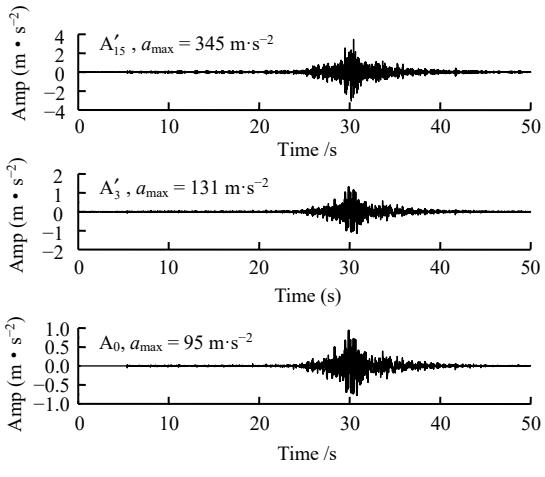

(b) Non-fissure slope

Fig. 5 Responses of slope monitoring points under the action of horizontal Tangyu wave

This paper mainly explores the dynamic response law of two slopes on loess tableland from the slope surface and internal vertical section. To facilitate comparison, the dimensionless acceleration amplification factor M_{PGA} is introduced. The ratio of peak acceleration of measuring point to the peak acceleration of A_0 on the table is defined as PGA amplification factor. The distribution law of the amplification factor represents the distribution law of acceleration.

3.1 Acceleration response on slope surface

Figures 6 and 7 show the PGA amplification factor of the slope surface under horizontal and vertical seismic motions. It can be seen the PGA amplification factors of the slope surfaces of two structures show obvious nonlinear in elevation, and the distribution of acceleration on the slope has rhythm, that is, with the increase of elevation, the PGA amplification factor is basically increasing. At the same time, the slope structure has selectivity to the amplification of horizontal acceleration. When the measuring point is located below the fissure, the PGA amplification factor of the non-fissure slope is slightly larger than that of the fissure slope at the same height. When the height increases to the elevation of the fissure (H = 0.8 m), the PGA amplification factor curve of the fissure slope increases suddenly, while the increase rate of the non-fissure slope at this location does not change significantly. And the PGA amplification factor of the fissure slope is obviously larger than that of the non-fissure slope at the top of the slope. For example, the amplification factors of fissure slope at the top of slope are 4.0 and 3.9 under the horizontal Tangyu motions with PGA values of 355 and 517 cm·s^{-2}(as shown in Figs. 7(a) and 7(b)); however, the corresponding amplification factors at the top of the non-fissure slope are 3.3 and 3.4, increasing by 21% and 15%, respectively. At the same time, the two slopes show the surface effect. The closer to the slope surface and the top of the slope, the more obvious the amplification effect is.

By selecting Tangyu wave and El-Centro wave with the same amplitude, it is found that the amplification effect of Tangyu motion is generally greater than that of El-Centro motion, and the reason for this phenomenon may be related to the frequency distribution of Tangyu wave. According to the numerical simulation analysis, the natural frequencies of the fissure slope and non-fissure slope are 17.4 Hz and 18.9 Hz, respectively. The spectrum amplitudes of Tangyu motion near these two frequencies are stronger than those of El-Centro motion, which leads to the more intense dynamic response of the slope when Tangyu motion is loaded.

It can be found from Figs. 6 and 7 that the seismic motions input in the x-direction and z-direction show obvious amplification effect along the elevation, At the same time, the PGA amplification factor are abruptly changed at the fissure, but no obvious mutation occurs at the slope without fissure. By comparing the motions with similar amplitudes but different directions, it is found that the amplification factor of x-direction motion near

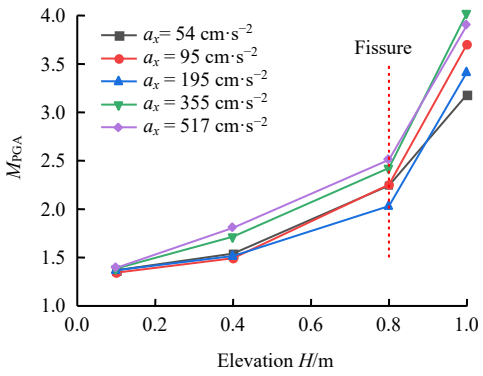

(a) Dynamic response of fissure slope under x-direction seismic motion

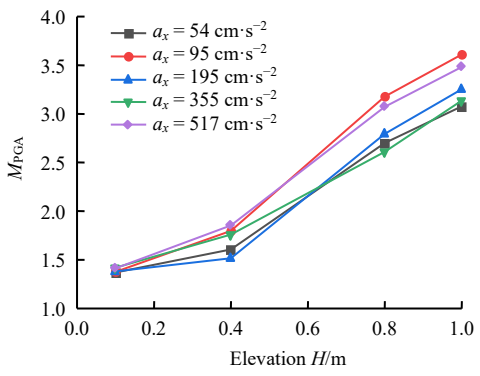

(b) Dynamic response of non-fissure slope under x-direction seismic motion

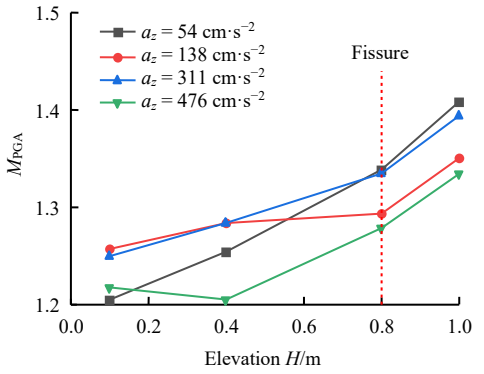

(c) Dynamic response of fissure slope under z-direction seismic motion

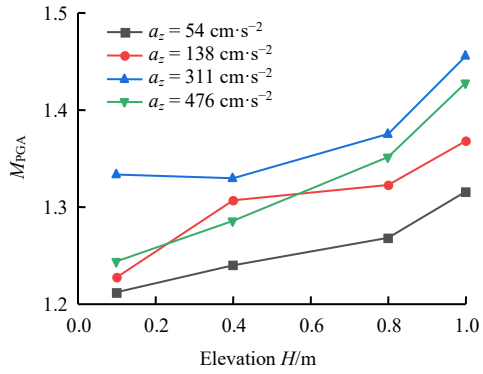

(d) Dynamic response of non-fissure slope under z-direction seismic motion

Fig. 6 PGA amplification coefficients of slope monitoring points under Tangyu wave in different directions

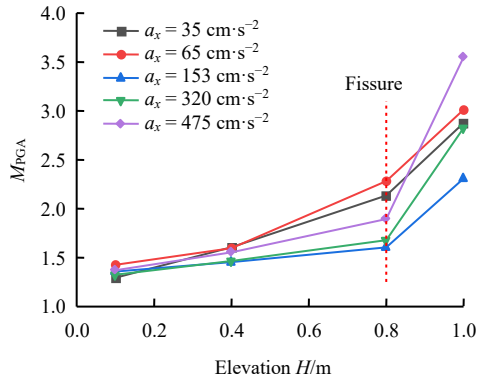

(a) Dynamic response of fissure slope under x-direction seismic motion

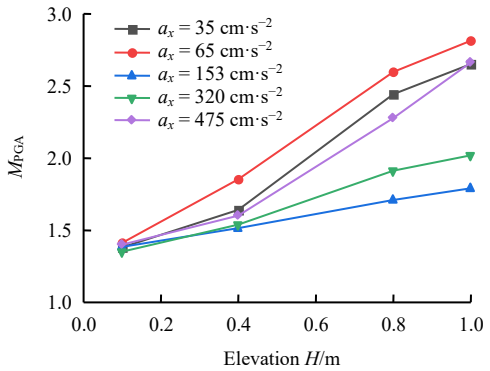

(b) Dynamic response of non-fissure slope under x-direction seismic motion

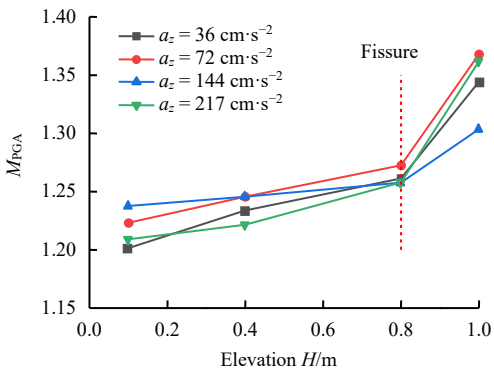

(c) Dynamic response of fissure slope under z-direction seismic motion

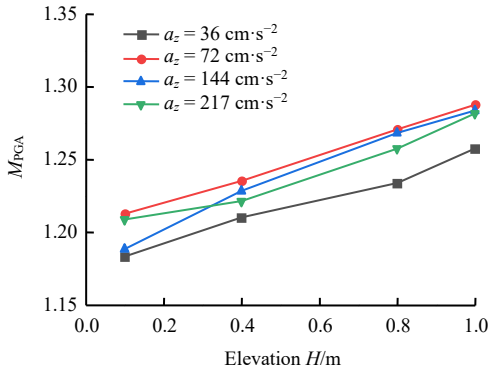

(d) Dynamic response of non-fissure slope under z-direction seismic motion

Fig. 7 PGA amplification coefficient of slope monitoring points under the El-Centro motion in different directions

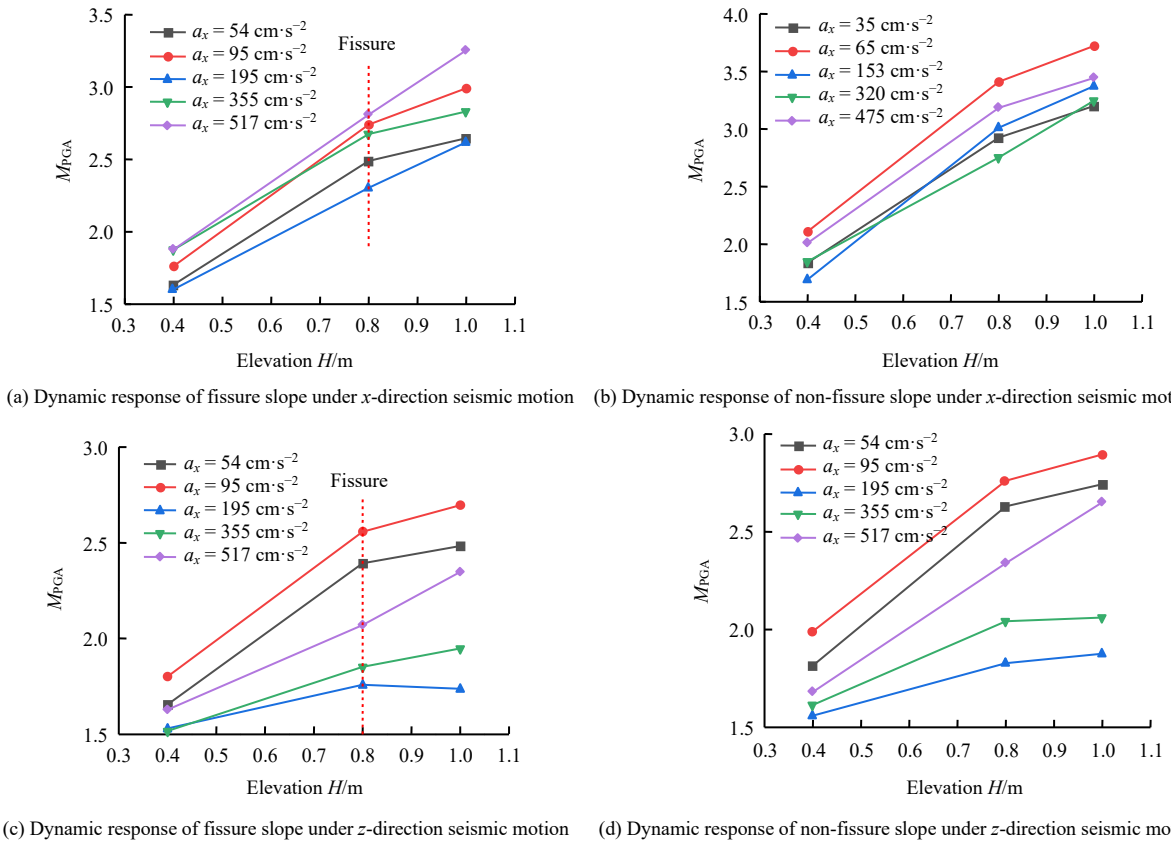

(a) Dynamic response of fissure slope under x-direction seismic motion (b) Dynamic response of non-fissure slope under x-direction seismic motion

(c) Dynamic response of fissure slope under z-direction seismic motion (d) Dynamic response of non-fissure slope under z-direction seismic motion

Fig. 8 PGA amplification coefficient of monitoring points in section 1 under the action of different types of seismic motions

the top of slope is significantly larger than that of z-direction motion, and it is about 2 times. The results show that the horizontal motion has a greater influence on the dynamic stability of the slope. It further verifies that the horizontal motion in natural earthquakes may be the main reason of the slope failure on the loess tableland.

3.2 Acceleration response of section 1

Figure 8 shows the amplification factor of two slopes in section 1 under horizontal motion. It can be noted that the PGA of the two slopes in section 1 and the slope surface have similar laws, both show a nonlinear increasing trend with the maximum value at the top of the slope. But the difference is that the amplification factor curve near the fissure in section 1 decreases rapidly compared with the slope surface, and the PGA of the fissure slope at the same height is smaller than that of the non-fissure slope.

Since the reflection mechanism of seismic waves and the low-density soil near the fissure absorb most of the energy, the fissure becomes a barrier to block the propagation of seismic motion, which greatly reduces the energy behind the fissure. In addition, the existence of fissure has a complex influence on wave propagation, and the PGA amplification factors of vertical seismic waves in section 1 and slope face have similar laws. In order to save space, they will not be listed here.

3.3 Acceleration response of section 4

Fig. 9 shows the amplification factor of horizontal motion on the section 4 of two slopes. It can be seen the trends of PGA amplification factor on the section 4 and slope surface are similar. However, compared with other positions, the sudden increase in amplification factor of section 4 near the fissure is the most significant(the ratios of the amplification factor of the A15, A12, and A14 on the top surface to the measuring points A11, A16, A10, are 1.45, 1.15, 1.63, respectively), and the PGA amplification factor at the measuring point A14 on the top surface is also greater than those of A15 of the slope surface and A12 of the section 1. Because the fissures cut the upper slope into three blocks, and the fissure continue to expand and extend under the loading of seismic motions, finally, the stiffness decreases. Due to the existence of free surface, the bending stiffness of the outermost block decreases mostly(unless there are factors such as large volume deformation or water absorption). In addition, due to the difference of media between the two sides, seismic motion will produce reflected wave and transmitted wave at the interface, which leads to a significant interface dynamic effect.

Based on the comprehensive analysis of the response analysis of the slope at 3 locations, it is found that the PGA amplification factor from the front edge to the rear edge of the non-fissure slope shows an attenuation law,

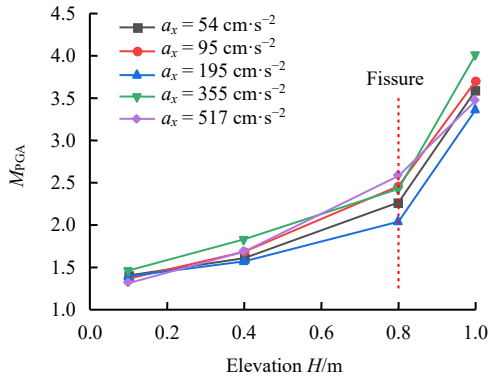

(a) Dynamic response of fissure slope under x-direction seismic motion

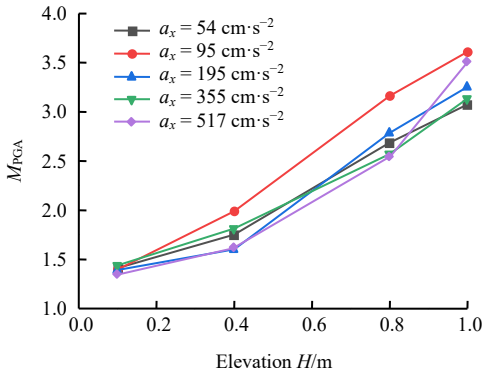

(b) Dynamic response of non-fissure slope under x-direction seismic motion

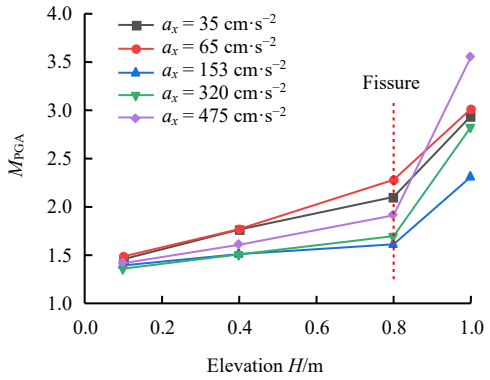

(c) Dynamic response of fissure slope under z-direction seismic motion

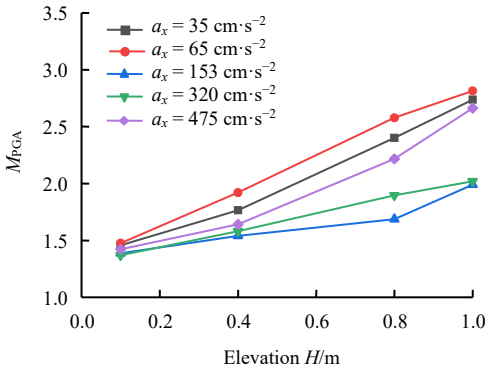

(d) Dynamic response of non-fissure slope under z-direction seismic motion

Fig. 9 PGA amplification coefficients of monitoring points in section 4 under different types of seismic waves

which is consistent with the numerical simulation results of Wang et al.[20]. Because of the existence of fissures, the acceleration response near the fissure on the top surface is the largest, followed by the slope surface and the back edge of the slope. Therefore, from the perspective of acceleration response, the non-fissure slope is first destroyed from the front edge of the slope, the fissure slope is first destroyed from the fissure, and then expands to both sides of the fissure.

4 Spectrum analysis

This chapter mainly focuses on the frequency of seismic motions. The Fourier spectrum is smoothed properly on the premise of not changing the basic shape of the spectral line in order to explore the possible reasons for the difference of acceleration response. At the same time, the spectrums of El-Centro motion and Tangyu motion have similar characteristics. Figures 10 and 11 mainly take El-Centro motion as an example to analyze the changes in the shape and amplitude of the spectral lines after seismic motions propagate through the medium.

Figure 10 illustrates the Fourier spectrum at the measuring points on the slope surface under the loading of horizontal El-Centro motion. The magnitude of the amplitude in the Fourier spectrum represents the amount of accumulated energy, and the amplitude difference between the spectral lines represents the change of energy between the monitoring points when the seismic wave passes through different parts of the slope. It can be seen from the figure that the spectral line shape of different measuring points has certain similarity with the increase of height. In the upper part of the slope, the primary frequency of A_{15} has large amplitude, and the amplitude difference between A_{11} and A_{15} is larger. However, in the lower part of the slope, the larger amplitude appears at the measuring points on the side of the non-fissure slope. The amplification factor in the lower part of the non-fissure slope and the upper part of the fissure slope is larger, which verifies the conclusion of section 3.1.

When the horizontal acceleration is 35 cm·s^{-2}, as shown in Fig. 10(a) and Fig. 10(d), the primary frequencies of A_3 and A_7 at the lower part of the slope are mainly distributed around 5 Hz, while the primary frequencies of A_{11} and A_{15} are mainly distributed in the high frequency band of 23 Hz. In other words, with the increases of elevation, the slope will selectively amplify the mid-high frequency range. When the acceleration is 35 cm·s^{-2}, the predominant frequency of the slope is distributed around 23 Hz, and the amplitude is small. However, when the acceleration amplitude increases to 320 cm·s^{-2}, the predominant frequency of the slope attenuates to 12 Hz, and its amplitude increases by about 4 times compared

with the loading of 35 cm·s^{-2}. At the same time, a second dominant frequency of 18 Hz appears. When the amplitude is 475 cm·s^{-2}, the amplitude of the primary frequency and the second dominant frequency increase, while the primary frequency attenuates to 10 Hz, and the value of the second dominant frequency basically maintains at 18 Hz. The frequency attenuation of non-fissure slope also has a similar law, the primary frequency of slope decreases with the increase of amplitude, and approaches the dominant frequency of the seismic motions.

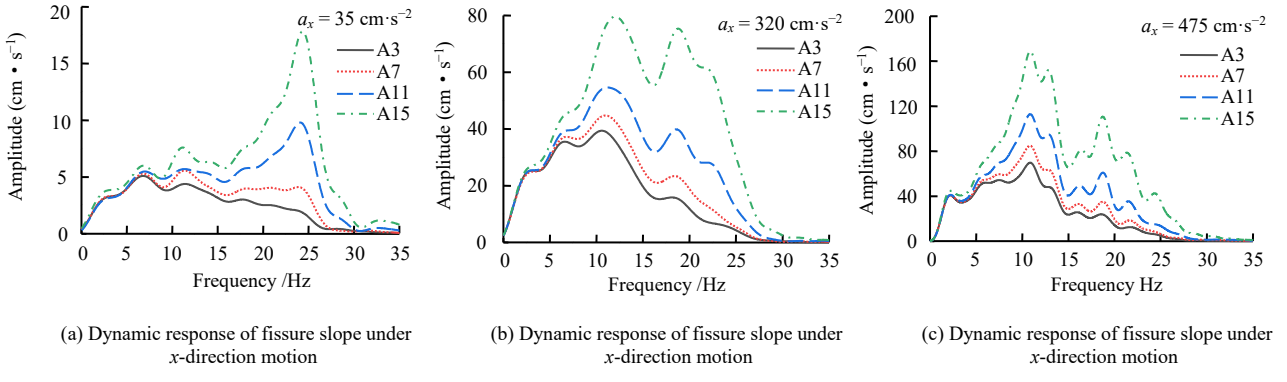

(a) Dynamic response of fissure slope under *x*-direction motion (b) Dynamic response of fissure slope under *x*-direction motion (c) Dynamic response of fissure slope under *x*-direction motion

(d) Dynamic response of non-fissure slope under *x*-direction motion (e) Dynamic response of non-fissure slope under *x*-direction motion (f) Dynamic response of non-fissure slope under *x*-direction motion

Fig. 10 Acceleration Fourier spectrum of monitoring points on slope under the horizontal El-Centro motion

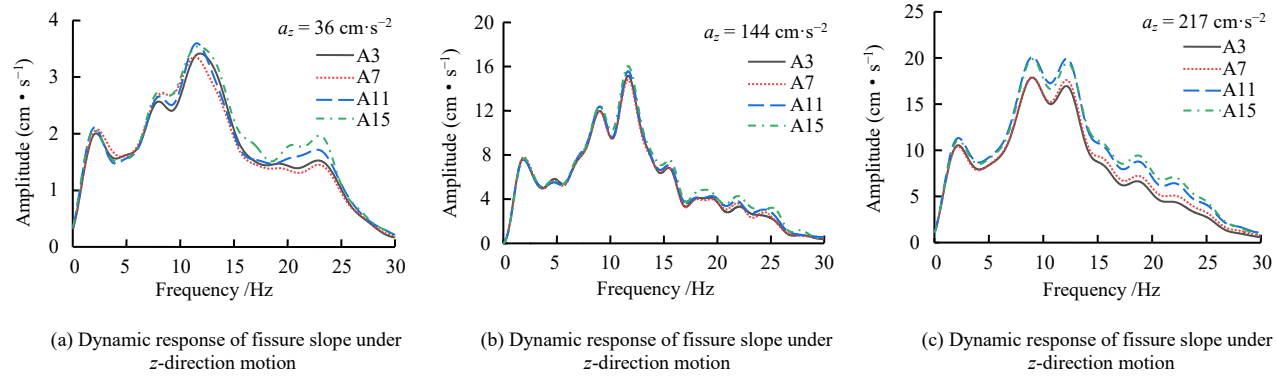

(a) Dynamic response of fissure slope under *z*-direction motion (b) Dynamic response of fissure slope under *z*-direction motion (c) Dynamic response of fissure slope under *z*-direction motion

(d) Dynamic response of non-fissure slope under *z*-direction motion (e) Dynamic response of non-fissure slope under *z*-direction motion (f) Dynamic response of non-fissure slope under *z*-direction motion

Fig. 11 Fourier spectrum of acceleration at each monitoring point on the slope under vertical El-Centro wave in *z* direction

Figure 11 analyzes the response characteristics of Fourier spectrum under the loading of vertical El-Centro motion, and compares them with the Fourier spectrum under horizontal motion. The similarities and differences are summarized as follows:

(1) Under the same acceleration amplitude, the shape of Fourier spectra at different elevations are very similar. Compared with the Fourier spectrums under horizontal seismic waves, the amplitudes of spectrum under vertical seismic waves are smaller, and the amplitudes at different elevations are close. There is almost no altitude effect.

(2) Under the vertical seismic waves, the predominant frequency of El-Centro wave is basically maintained at 12 Hz. As the amplitude increases, the predominant frequency increases slightly and hardly attenuates.

(3) Under the vertical seismic waves, the existence of fissure has no significant effect on the Fourier spectrum of two kinds of slopes. Compared with the horizontal motion of the same amplitude, the vertical motions has less influence on the dynamic response of the slopes.

According to the comprehensive analysis of the Fourier spectrum, it is found that the amplification effect of acceleration along the elevation is dependent on a certain frequency band, which is related to the size and stiffness of the model slope. In the fissure slope, the location of fissure (H > 0.8 m) is the most significant part, which makes the PGA amplification change suddenly with the increase of elevation. However, the PGA amplification of the non-fissure slope is not significantly affected, and almost linearly increases. With the loading of seismic motion, dislocation occurs between soil particles, and the plastic work consumes part of the energy of the wave and generates heat. In the vertical direction, due to the small constraint on the upper slope and the superimposition of seismic motions, large displacement response will generate in the slope, and the mechanical properties of soil will be damaged gradually. Damage is an irreversible energy conversion process, which increases the energy consumption of seismic motions[21]. As the amplitude of seismic motions increases, the dissipated energy increases, and the damage increases further, which makes the stiffness decrease and the primary frequency decrease. Finally, the seismic motions of high frequency component of slope attenuate faster. As can be seen from Fig.10, the attenuation of high-frequency components become more obvious with the increase of amplitude.

5 Conclusion

In this paper, the shaking table tests of fissure slope and non-fissure slope are completed. By applying Tangyu and El-Centro motion with different amplitudes, the response law of x-direction and z-direction seismic motions is discussed. Following by an analysis of Fourier spectrum of different kinds of slopes. The following conclusions are obtained as follows:

(1) The PGA amplification effect of the two slopes on the slope surface and internal vertical section shows the elevation amplification effect. The closer to the slope surface and the top of slope, the more obvious the amplification effect is. And the amplification effect of horizontal motion on slope is greater than that of the vertical motion under the same amplitude of seismic waves.

(2) The existence of fissures has an important influence on the propagation and the dynamic response in the slope. The test results show the response of slope surface and section 4 of fissure slope is significantly greater than that of non-fissure slope in the upper part of the slope. When the wave propagates near the fissure in Section 4, due to the difference between the media on both sides of the fissure, significant interfacial dynamic effect generates, which directly lead to reflection and refraction near the fissure. However, Section 1 is located at the back of the slope, and the fissure becomes a barrier to block the propagation of wave, which greatly attenuates the energy transmitted into the back side, resulting in the response of section 1 lower than that of the non-fissure slope. The response law of two slopes on slope surface and vertical section is similar under the action of z-direction seismic.

(3) The predominant frequency of the wave has a significant change after being transmitted through the soil medium. With the increase of the elevation, the slope can selectively amplify some frequency bands, which will be more obvious on the fissure slope. When the amplitude continuously increases, the primary frequency shifts to the low frequency direction, but its spectral amplitude continues increase. The shapes of Fourier spectrum at different elevations are very similar under the vertical seismic wave. Compared with the Fourier spectrum under horizontal seismic wave, the spectrum amplitude under the vertical seismic wave is smaller, and the amplitudes of the measuring points at different elevations are close. There is almost no altitude effect, meanwhile, the predominant frequency does not attenuate significantly.

References

[1] XIN Hong-bo, WANG Yu-qing. Earthquake-induced landslide and avalanche[J]. Chinese Journal of Geotechnical Engineering, 1999, 21(5): 591−594.

[2] WANG Lan-min, SHI Yu-cheng, LIU Xu, et al. Loess

dynamics[M]. Beijing: Seismological Press, 2003.

[3] Lanzhou Institute of Seismology, State Seismological Bureau. Catalogue of strong earthquakes in four provinces(regions) of Shanxi, Gansu, Ningxia and Qinghai[M]. Xi'an: Shaanxi Science and Technology Press, 1985.

[4] WEN B, WANG S, WANG E, et al. Characteristics of rapid giant landslides in China[J]. Landslides, 2004, 1(4): 247−261.

[5] ZHUANG J Q, PENG J B, XU C, et al. Distribution and characteristics of loess landslides triggered by the 1920 Haiyuan Earthquake, Northwest of China[J]. Geomorphology, 2018, 314(Aug.1): 1−12.

[6] BOUCKOVALAS G D, PAPADIMITRIOU A G. Numerical evaluation of slope topography effects on seismic ground motion[J]. Soil Dynamics and Earthquake Engineering, 2005, 25(7−10): 547−558.

[7] QI Sheng-wen. Two patterns of dynamic responses of single-free-surface slopes and their threshold height[J]. Journal of Geophysics, 2006, 49(2): 518−523.

[8] JIANG Ming-jing. New paradigm for modern soil mechanics: geomechanics from micro to macro[J]. Chinese Journal of Geotechnical Engineering, 2019, 41(2): 195−254.

[9] WU Zhi-jian, LEI Tian, CHEN Yu-jin, et al. deformation and instability characteristics of loess slope base on shaking table model[J]. Journal of Shanghai Jiaotong University, 2015, 49(7): 940−945.

[10] WANG Lan-min, PU Xiao-wu, WU Zhi-jian, et al. Shaking table tests of dynamic response of loess slopes under the coupling effects of earthquake and rainfalls[J]. Chinese Journal of Geotechnical Engineering, 2018, 40(7): 1287−1293.

[11] ZHANG Z, WANG T, WU S, et al. Seismic performance of loess-mudstone slope in Tianshui-centrifuge model tests and numerical analysis[J]. Engineering Geology, 2017, 222: 225−235.

[12] WU Z, ZHAO D, CHE A, et al. Dynamic response characteristics and failure mode of slopes on the loess tableland using a shaking-table model test[J]. Landslides, 2020, 17(7): 1561−1575.

[13] WU Z J, ZHANG D, WANG S N, et al. Dynamic-response characteristics and deformation evolution of loess slopes under seismic loads[J/OL]. Engineering Geology, 2020, 267: https://doi.org/10.1016/j.enggeo.2020.105507.

[14] XIAO Wen-jing, LIAO Jia-ming, ZHANG Liang-liang. Shaking table test on seismic dynamic responses of isolated mountains[J]. Earthquake Engineering Journal, 2018, 40(3): 582−590.

[15] ZHU Ren-jie, CHE Ai-lan, YAN Fei, et al. Dynamic evolution of rock slope with connective structural surface[J]. Rock and Soil Mechanics, 2019, 40(5): 1907−1915.

[16] LIU Han-xiang, XU Qiang, ZHU Xing, et al. Marginal spectrum characteristics of the rock slope with a soft interlayer during an earthquake[J]. Rock and Soil Mechanics, 2019, 40(4): 1387−1396.

[17] LU Xi-lin, CHEN Yue-qing, CHEN Bo, et al. Shaking table test of dynamic soil-structure interaction system[J]. Seismic Engineering and Engineering Vibration, 2000, 20(4): 20−29.

[18] YUAN Wen-zhong. Similar theoretical and static model test[M]. Chengdu: Southwest Jiaotong University Press, 1998.

[19] LIN Gao, ZHU Tong, LIN Bei. Similarity technique for dynamic structural model test[J]. Journal of Dalian University of Technology, 2000, 40(1): 1−8.

[20] WANG L M, WU Z J, XIA K, et al. Amplification of thickness and topography of loess deposit on seismic ground motion and its seismic design methods[J]. Soil Dynamics and Earthquake Engineering, 2019, 126.

[21] LEMAITRE J, SERMAGE J P, DESMORAT R. A two scale damage concept applied to fatigue[J]. International Journal of Fracture, 1999, 97(1): 67−81.